Detection and Correction of Patient Motion in Dynamic and Static Myocardial SPECT Using a Multi-Detector Camera

Guido Germano, Terrance Chua, Paul B. Kavanagh, Hosen Kiat and Daniel S. Berman

Department of Medical Physics and Imaging, Division of Nuclear Cardiology, Department of Medicine, and Division of Nuclear Medicine, Department of Imaging, Cedars-Sinai Research Institute, Cedars-Sinai Medical Center; and Division of Nuclear Medicine, Department of Radiological Sciences, and Department of Medicine, UCLA School of Medicine, Los Angeles, California

We have developed a method for the detection and correction of translational patient motion in dynamic and static myocardial SPECT studies. The method uses a low activity ^{99m}Tc point source and is especially designed for multi-detector cameras. The source's centroid coordinates are measured or derived for all projection images in a temporal frame. The coordinate curves fitted to predicted distributions and the projection images shifted to realign measured to fitted values, with sub-pixel accuracy. In dynamic studies, the frame with the best fits serves as reference for all others. The accuracy of this method, measured with cardiac phantom experiments, was found to be ±0.37 mm and ±0.44 mm in the axial and transaxial dimension, respectively. By comparison, overall motion in 42 patients undergoing ^{99m}Tc-teboroxime dynamic cardiac SPECT studies was ±1.6 mm and ±1.2 mm, respectively (average on 39,272 projection views). Application of the method to phantom experiments, ^{99m}Tc-sestamibi and ^{99m}Tc-teboroxime human studies visually eliminated artifactual perfusion defects from simulated phantom motion and actual patient motion.

J Nucl Med 1993; 34:1349–1355

Dynamic SPECT studies are defined as a succession of temporal frames, where a temporal frame(s) is a complete set of projection images (also planar images, raw images, planar views), acquired over 180° or 360°. A static SPECT study consists of one temporal frame comprising multiple planar images. In contrast, in static or dynamic planar studies, one temporal frame coincides with a single planar view.

Artifacts and inaccuracies due to patient or organ motion are well documented in the nuclear medicine literature (*1–4*). The effect of mild motion is loss of resolution or blurring of planar and SPECT images, with consequent loss of contrast in areas of abnormally low (defects) or high (hot spots) isotopic uptake. In more extreme cases, motion can create artifactual defects or hot spots or distort the images so as to render them uninterpretable. Motion-correction algorithms have been developed for a variety of dynamic planar nuclear medicine studies. In hepatic scintigraphy, the change in the center of mass position of the liver was used as an index of liver motion (*5*), and analog motion correction circuitry was employed to reposition the center of hepatic radionuclide activity at regular time intervals (*6–8*). In another approach, the data was handled and filtered in the Fourier or frequency domain (*9*). In dynamic renal scintigraphy, organ motion was compensated for by securing two ^{57}Co point sources to the patient, tracking their position during the study and shifting the images to match the sources' baseline position (*10*). Alternatively, a maximum count-based iterative algorithm automatically repositioned two regions of interest (ROIs) encompassing the kidneys, frame after frame (*11*).

Point sources have also been used in cardiac gated exercise blood pool studies (*12*) and first-pass radionuclide angiography (*13*). In these studies, motion correction algorithms tracking the heart's center of mass are not as effective because cardiac contractions and rotations mask the actual patient motion. Motion correction in ^{201}Tl myocardial SPECT studies has been implemented to address the problem of the upward creep of the heart following exercise, a phenomenon first recognized by Friedman et al. (*14*). In one approach, upward heart motion was detected by fitting a straight line to the upper and lower border of projection images from early and late frames of ^{201}Tl studies (*15*), and interpolative correction effected by interpolation. In static SPECT studies, axial patient motion was detected through analysis of the cross-correlation functions between adjacent planar views (*16*) or by calculating the center of the mass of the heart and mapping its position over all planar views (*17*).

The purpose of this study was to devise a motion detection and correction technique for static and dynamic myocardial SPECT studies using ^{99m}Tc agents, a technique

Received Dec. 10, 1992; revision accepted Mar. 18, 1993.

For correspondence and reprints contact: Guido Germano, PhD, Director, Nuclear Medicine Physics, Cedars-Sinai Medical Center A047 N, 8700 Beverly Blvd., Los Angeles, CA 90048.

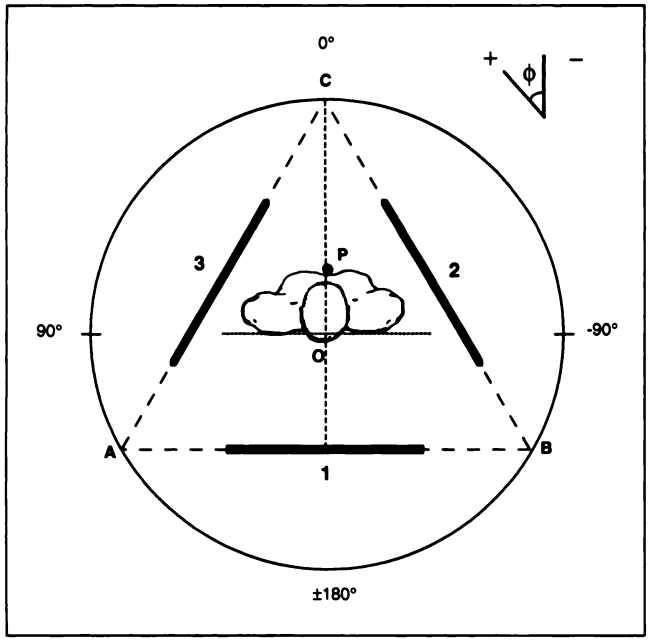

FIGURE 1. Schematic diagram of a triple-detector camera acquisition setup. P is the point source marker, O the center of rotation of the detector assembly and 1, 2 and 3 the detector planes, in section. The "angle" ϕ of a detector during rotation is defined as the angle between the perpendicular to its back surface (the one away from the patient) and PC. The circle in figure would be described by points A, B and C in a circular acquisition.

especially designed to fully exploit the capabilities of multi-detector SPECT cameras.

THEORY

Let us assume that the initial position of the three detector planes 1, 2 and 3 in a triple-detector camera is that shown in Figure 1. A 360° frame is acquired by rotating each detector around the patient along a 120° arc, whose radius is the starting distance between the detector and the center of the field of view (O in Fig. 1). In circular acquisition, all the radii have the same value while in contoured acquisition, the values are variable along the arc to reduce the collimator-to-patient distance and achieve better resolution. The "angle" ϕ of a detector during rotation is defined as the angle between the perpendicular to its back surface (the one away from the patient) and the 12 o'clock line (PC in Fig. 1). We shall define this angle as positive in a manner consistent with counter-clockwise (CCW) rotation, which is the default rotation for the first frame of a study acquired on our camera. P is a point source marker, which in Figure 1 is positioned on the sternal region of an imaginary patient. Figure 2 exemplifies the projection angles covered by each detector during a frame acquired with alternating CCW and clockwise (CW) rotations. The shaded areas represent the angular range (−90° to 90° if the source is not active enough to shine through the patient) over which the point source marker is "seen" on the projection images. Reconstruction over 180° is generally performed using the projection data between −45° and −135°; thus, the source is not seen by Detector 3 in the angular

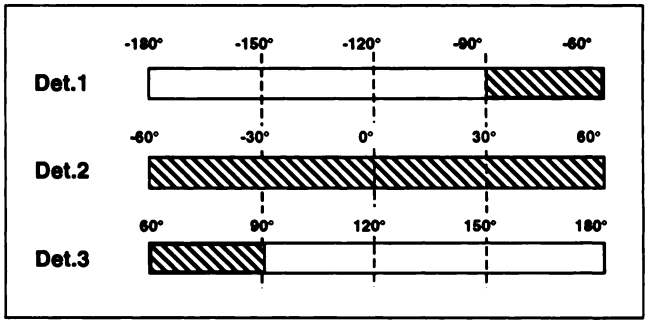

FIGURE 2. Projection angles covered by detector 1, 2 and 3 during a frame acquired with counter-clockwise rotation (frame duration = T). The hashed areas represent angles at which a relatively weak source would be "seen" in the corresponding projection images.

interval (90°, 135°). In order to correct those projections for motion, one can use the interval (−30°, 15°) simultaneously scanned by Detector 2.

For translational source motion, i.e., motion in the plane containing the source and parallel to the room floor, any motion in that plane can be decomposed into an axial (parallel to the axis of rotation of the detector assembly) and transaxial component, which shall be termed Δy and Δx, respectively. If the detectors are well aligned, axial motion will appear equally on all three detectors, and in particular:

$$\Delta y_3|_{(\alpha^\circ)} = \Delta y_2|_{(\alpha^\circ - 120^\circ)} \qquad \alpha \in (90^\circ, 135^\circ), \quad \text{Eq. 1}$$

where, with $\Delta y_3|_{(\alpha^\circ)}$, we have indicated Δy as seen on the α° projection collected by Detector 3.

The relationship between transaxial motion components on adjacent detectors is exemplified in Figure 3. Trigonometrically,

$$\Delta x_2 = \Delta x \cos \phi \quad ; \quad \Delta x_3 = \Delta x \cos \vartheta, \quad \text{Eq. 2}$$

and since

$$\vartheta = 60^\circ - \phi, \quad \text{Eq. 3}$$

it descends that

$$\Delta x_3 = \Delta x_2 \frac{\cos (60^\circ - \phi)}{\cos \phi} \qquad \phi \in (-30^\circ, 15^\circ).$$

Eq. 4

MATERIALS AND METHODS

A triple-detector camera (Prism 3000, Picker, Cleveland, OH) with LEHR collimators was used for all patient and phantom studies. A 2 × 2 mm^2 point source was manufactured in-house for each study by placing a drop of ^{99m}Tc (approximate activity 100 μCi) on a vial cap then sealing the cap with adhesive tape. In human studies, the point source was taped to the patient's sternum, a few centimeters above the heart, to ensure good contrast. The overall patient's skin dose from the source is about 5 mrad (*10*) and the source-produced scatter to the myocardium was measured and found lower than 1% of the myocardial activity in ^{99m}Tc-teboroxime and ^{99m}Tc-sestamibi studies. Static SPECT

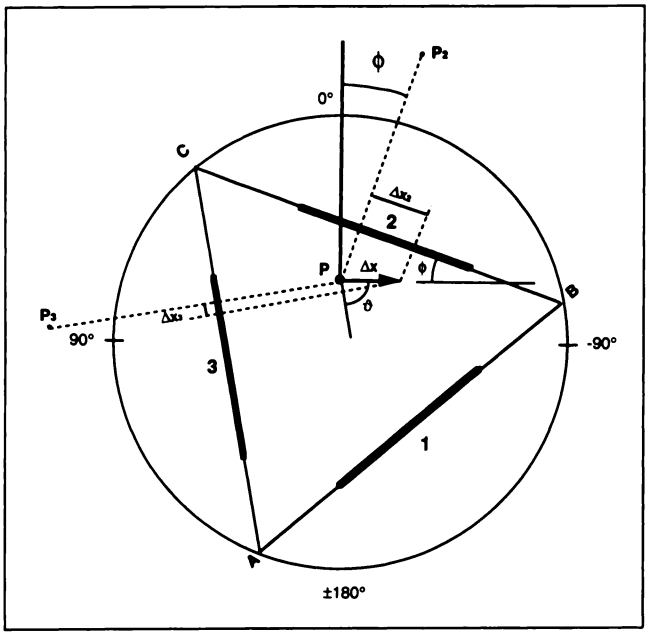

FIGURE 3. If the source P moves transaxially by an amount Δx, its unknown component Δx_3 on detector 3 can be derived from the simultaneously measured component Δx_2 on detector 2. From simple trigonometric considerations, it descends that $\Delta x_3 = \Delta x_2 (\cos (60° - \phi)/\cos \phi)$.

studies were acquired with continuous CCW rotation, dynamic SPECT studies with continuous, alternating CCW and CW rotation. All studies were acquired and reconstructed in 64 × 64 pixels^2 matrices.

Marker's Centroid Determination

Figure 4 shows a typical projection image of a commercial chest phantom (Data Spectrum 2230 with Cardiac Insert 7070, Chapel Hill, NC), the point source and a crosshair which is automatically superimposed on all images, about one-third from the top of the images. All projections in a frame are simultaneously displayed to the operator, who positions the crosshair to make it the lower boundary of a rectangle within which the source is the highest activity structure. For each projection, the program then automatically finds the maximum pixel value $P(x_0, y_0)$ above the crosshair. The pixel counts for the image row through that pixel are histogrammed, the histogram's median is taken as a measure of the background (Bkg) and a rectangle is defined by expanding left, right, up and down from (x_0, y_0) until

$$P(x, y) < 0.3(P(x_0, y_0) - Bkg). \quad \text{Eq. 5}$$

Additional constraints ensure that no rectangle side be larger than 10% of the image matrix size (5% from (x_0, y_0) in either direction). Moreover, the rectangle's bottom side cannot be lower than the crosshair. The background value is subtracted from all pixels within the rectangle, whose rows are then summed together and fitted to a Gaussian curve. The Gaussian peak is the x-coordinate of the source's centroid. Repetition of same process for the axial dimension yields the y-coordinate of the source's centroid.

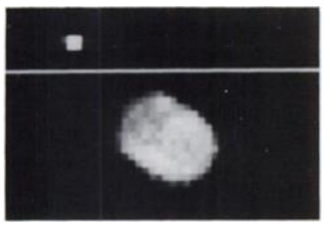

FIGURE 4. Typical projection image of a commercial chest phantom, the point source and a crosshair, which is automatically superimposed on all images by the motion correction software.

Iterating the procedure for all projections in a frame where the source is visible produces two curves, which express the x- and y-coordinate of the source's centroid as a function of the projection angle. These entire two curves, or a portion of them, can be fit to a sinusoid (x) and a line (y) which are the expected ideal distributions in the absence of motion. The product of the correlation coefficients for the two fits is assumed to be a measure of the source's stillness during the frame. Therefore, the differences between $(x, y)_{measured}$ and $(x, y)_{fit}$ represent the amounts by which the relative projection images must be shifted to compensate for motion. If only part of the curve was fitted, the fit must be extrapolated to cover the entire curve's angular range. Fractional pixel shifting of images is achieved through bilinear interpolation. In dynamic teboroxime washout studies or in other studies where multiple frames are acquired, the x and y fits for the frame with the least amount of motion (the one with the maximal correlation coefficients product) will serve as the reference to which all other frames are realigned, projection by projection.

Image Acquisition

Accuracy of Centroid Determination. To measure the accuracy of the centroid determination algorithm, a point source containing 100 μCi of ^{99m}Tc was placed in the camera's field of view (FOV) at the approximate location where it would be expected in a patient study. Forty 1-min frames of 120 projections each were acquired, center-of-rotation correction was applied and the differences between $(x, y)_{measured}$ and $(x, y)_{fit}$ for all frames were calculated and histogrammed into a "motion histogram."

Measurement of Individual and Average Patient Motion. A point source containing 100 μCi of ^{99m}Tc was placed on the sternum of 42 consecutive patients undergoing dynamic ^{99m}Tc-teboroxime myocardial SPECT, and 15–24 1-min frames consisting of 60 or 120 projections each were acquired as previously described (*18,19*). Center-of-rotation correction was applied and the differences between $(x, y)_{measured}$ and $(x, y)_{fit}$ for all frames were calculated and histogrammed into patient-specific motion histograms. To measure the average patient motion associated with this dynamic ^{99m}Tc-teboroxime protocol, all the individual histograms were also pooled together into a global motion histogram.

Motion Correction (Phantom). To test the theoretical basis of our motion correction algorithm, a chest phantom (Data Spectrum 2230 with Cardiac Insert 7070) was imaged over a 120 projections 3-min frame. The phantom's myocardium contained 400 μCi of ^{99m}Tc and a 4-cm^3 fillable chamber (*20*) to simulate a hypoperfused anterior defect. Projections corresponding to the last 90 sec of acquisition (−120° to −60°, 0° to 60° and 120° to 180°) were digitally shifted to simulate a sudden movement of 2 cm in the axial and 1 cm in the transaxial direction. The original data as well as the shifted data and the shifted data corrected for motion were reconstructed over 180° with a ramp filter and no attenuation correction.

Motion Correction (Clinical Data). To test the motion correction algorithm on clinical data, the method was applied to the twenty-four 1-min, 120 projection frames from the ^{99m}Tc-teboroxime study of a patient with a low likelihood of coronary artery disease (CAD) (*18*) and to the second of two 5-min, 120 projection frames from the ^{99m}Tc-sestamibi study of another patient. The first patient had been "a posteriori" determined to have moved

during the acquisition by motion histogram analysis (see Fig. 6); projection data frames 2–8 in the original and the motion-corrected set were summed to achieve good statistics, as described in (*18*), then the two summed sets were reconstructed and the resulting images compared. The second patient was prompted to move slightly up the bed (y direction) during acquisition of the second 5-min frame, then the original and motion-corrected versions of this frame were reconstructed and compared to the reconstructed, motion-free first frame. For both patients, data were prefiltered (Butterworth, order 5, cutoff frequency 0.215 of Nyquist) before reconstruction over 180° with a ramp filter and no attenuation correction.

RESULTS

Centroid Determination Accuracy

The discrete curves showing the x- and y-coordinates of the point source's centroid averaged over 40 frames were plotted as a function of the projection angle. As anticipated, it was possible to fit these curves to a sinusoid and a line, where the location of the line and the location, amplitude and phase of the sinusoid depend on the position of the point source in the camera's FOV. The differences between $(x, y)_{measured}$ and $(x, y)_{fit}$ for these data were histogrammed for all 40 frames over the angular range (−90°, 90°) (Fig. 5). Fitting these motion histograms to Gaussian distributions ($r > 0.99$, $p < 0.001$ for both fits) allows the calculation of $FWHM_x$ = 0.880 mm and $FWHM_y$ = 0.739 mm, which are measures of the method's accuracy.

Measure of Individual and Average Patient Motion

The same procedure was applied to data from the 42 dynamic ^{99m}Tc-teboroxime myocardial SPECT studies, resulting in 42 individual motion histogram pairs. One of these pairs is shown in Figure 6. In the absence of motion, one would expect the X and Y histograms to be Gaussian-like curves centered on the zero motion tick. In Figure 6, two additional peaks centered on +2.5 mm (x) and −3 mm (y) suggest that this patient moved by 2.5 mm and −3 mm in the x and y direction, respectively, spending some time at the new location. The global X and Y motion histograms (solid circles) and the relative Gaussian fits (solid lines) for the entire patient population are shown in Figure 7. The FWHM of the Gaussian curves are $FWHM_x$ = 4.295 mm and $FWHM_y$ = 3.130 mm, or five times larger than the correction method's accuracy. Thus, this motion correction method appears sensitive enough for use in the clinical practice of dynamic myocardial SPECT.

Motion Correction (Phantom)

Figure 8 shows reconstructed short-axis, mid-ventricular slices of the phantom with anterior defect. The simulated 1-cm (transaxial) and 2-cm (axial) shift of the phantom severely affects the quality and interpretability of the reconstructed images (left) with distortion of the left ventricular (LV) chamber and creation of an artifactual inferior/inferolateral defect in addition to the original "true" anterior defect. Application of our motion correction method to the shifted projection data results in reconstructed images (center) which are qualitatively identical to those reconstructed from unshifted projections (right), with only a slight loss of resolution due to sub-pixel interpolation. In studies with low-statistics, this smoothing effect may actually be desirable because it compensates for statistical noise in the image.

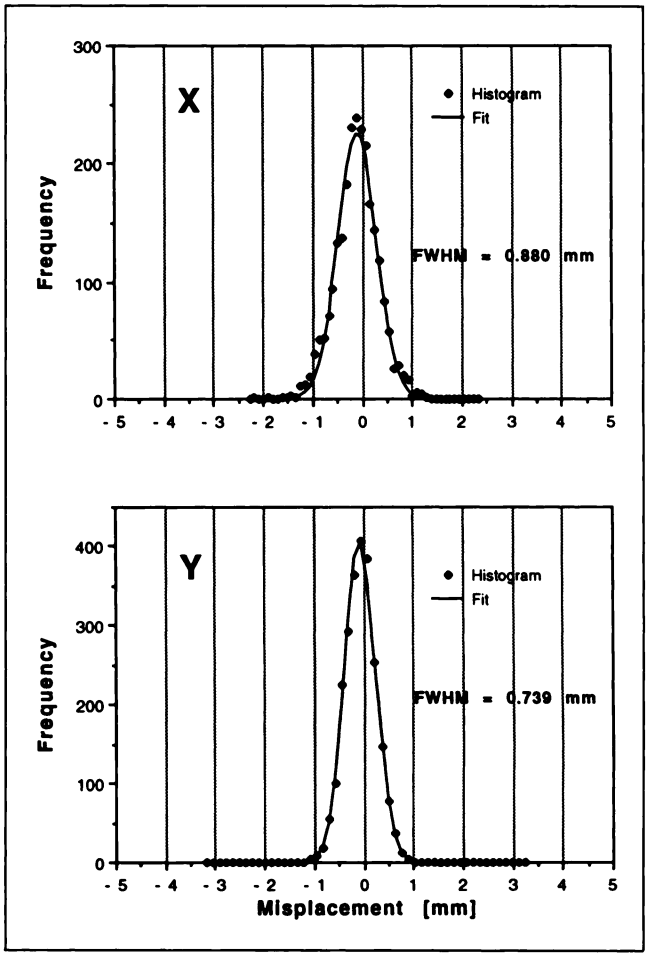

FIGURE 5. X and y motion histograms for the stationary phantom experiment calculated for all 40 frames over the angular range (−90°, 90°) (total projections = 2,400).

Motion Correction (Clinical Data)

Figure 9 shows reconstructed short-axis, mid-ventricular slices of the ^{99m}Tc-teboroxime patient with a low likelihood of CAD analyzed in Figure 6. The image reconstructed from the summed 2–8 min, motion-affected projection data demonstrates artifactual inferior and anterior perfusion defects (left). Correcting the projection data for motion before reconstruction restores a normal perfusion pattern (right). Figure 10 shows similar results for the ^{99m}Tc-sestamibi patient study. The motion-affected projection data are reconstructed into images with a distorted LV chamber as well as large anterior and inferior wall defects (left), whereas application of the motion correction method yields reconstructed images with a small inferior wall defect (center) and a perfusion pattern qualitatively identical to that in images reconstructed from the motion-free data (right).

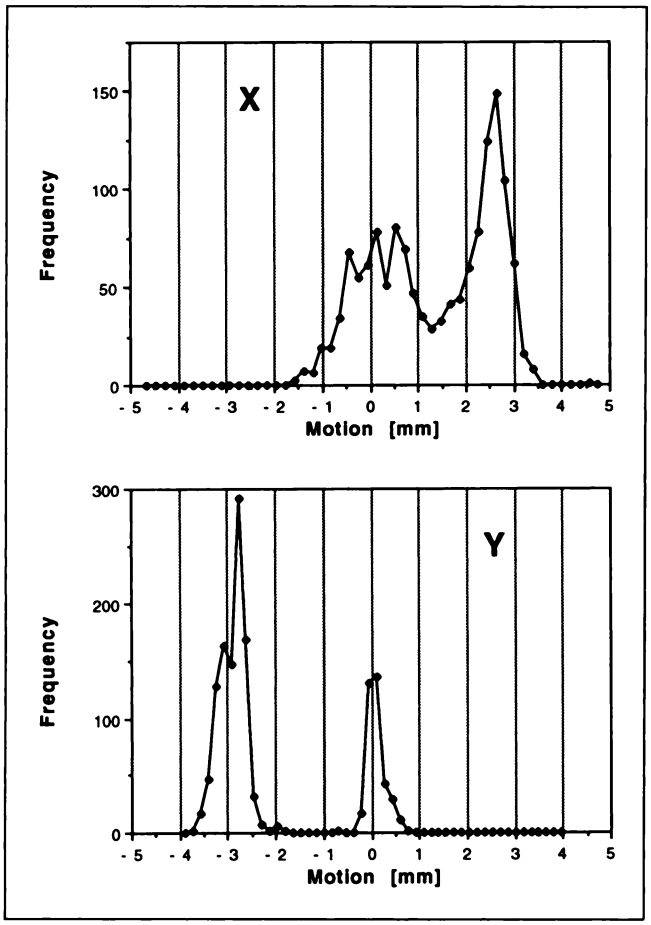

FIGURE 6. X and y motion histograms for an individual ^{99m}Tc-teboroxime patient calculated for 20 frames over the angular range (−90°, 90°). The presence of the two off-center peaks suggests that this patient moved by 2.5 mm and −3 mm in the x and y direction, respectively.

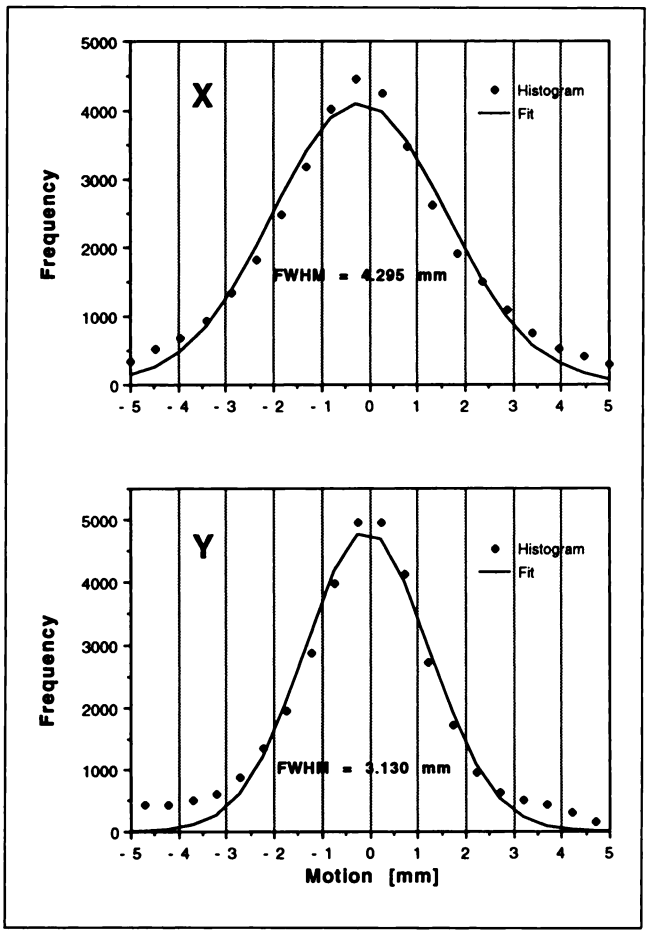

FIGURE 7. Global x and y motion histograms for the forty-two ^{99m}Tc-teboroxime patients calculated for all frames over the angular range (−90°, 90°) (total projections = 39,272).

DISCUSSION

We have presented a method for the detection and correction of translational patient motion in static and dynamic myocardial SPECT studies. The assumption that patient (thorax) motion can be well described by a point source secured to the patient's sternal region is supported by the virtual absence of muscle and fat on the sternum and the very low surrounding isotopic uptake. Independent source motion due to arm movement and related skin shifting should be negligible, since the patient's arms are immobilized over his/her head with our acquisition protocol (*18*). Alternative locations for the point source (i.e., the axillary cavity) were investigated and deemed susceptible to much greater spurious movements than the sternal region.

Gross heart motion is almost always due to patient motion (*17*), and its correction can dramatically improve the visual appearance and the interpretability of the reconstructed images; it must be noted, however, that some natural movements of the heart (e.g., postexercise upward creep or respiratory oscillations) are independent of patient motion. For rapid SPECT protocols with ~1 sec/projection (e.g., 1-min frames in ^{99m}Tc-teboroxime acquisition protocols) the heart cycle may not even be adequately integrated at each projection. In all of our studies, pharmacological stress was used and no upward creep of the heart was expected or seen; nonetheless, cine review of the projection data showed minor heart oscillations in 10%–20% of the studies, even after processing with our correction method. It is conceivable that a second correction for residual heart motion could be applied after correcting the data for patient motion. The potential benefits and risks of

FIGURE 8. Short-axis, mid-ventricular images reconstructed from shifted (left), shifted and corrected (center) and original unshifted (right) phantom projection data. Reconstruction of shifted data results in the distortion of the LV chamber and an artifactual inferior/inferolateral defect in addition to the original "true" anterior defect. Correction of shifted data results in images qualitatively identical to those reconstructed from the original data, with only a slight loss of resolution due to sub-pixel interpolation.

FIGURE 9. Dynamic ^{99m}Tc-teboroxime patient study contaminated by motion. The short-axis, mid-ventricular images reconstructed from summed, uncorrected projection data show artifactual inferolateral and anterior perfusion defects (left). Correcting for motion restores a normal perfusion pattern (right), with the slightly lower inferior wall uptake probably due to attenuation.

approaches based on center of mass tracking should, however, be carefully considered. Poor tracking of the heart's center and actual worsening of the images has been reported in rest or redistribution studies or for high liver-to-heart activity ratios in ^{201}Tl SPECT (*17*), and the minimal skeletal muscle hyperemia associated with pharmacological stressing results in even higher hepatic uptake than with exercise stressing. Technetium-99m-teboroxime poses special challenges in view of this agent's combination of high hepatic uptake and rapidly changing distribution pattern.

A possible extension of this work would employ two or three sources to detect motion in any direction. Problems in this approach are mainly connected to the selection of the optimal location(s) for the additional source(s). As a general rule, accuracy in detecting rotational patient motion would be proportional to the distance between point sources. On the other hand, the greater that distance, the less it can be assumed that the portion of the patient's body between the sources is completely rigid and consequently, the higher the error in the determination of the appropriate correction to apply. Tissue attenuation would also effectively prevent one from locating the sources both on the front and the back of the patient, unless activities much larger than 100 μCi are used. In order to minimize noise and reduce processing time—now about 15 sec/120 projections on an Odissey 1500 computer (Picker, Cleveland, OH), the standard platform for the Picker Prism 3000 camera—the algorithm could be modified so that only motion greater than the technique's accuracy be corrected by image shifting. Based on our phantom experiment, one would correct only motion of absolute value greater than FWHM/2, i.e., ±0.44 mm and ±0.37 mm for the transaxial and axial dimension, respectively. This strategy would still be capable of compensating for gross motion, a main concern in clinical practice and is consistent with the suggestion to employ a 0.5 pixel threshold (in a 64 × 64 matrix) when correcting for axial motion (*21*).

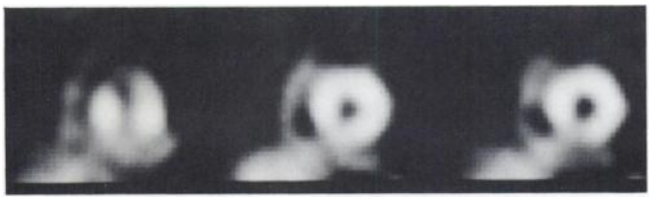

FIGURE 10. Static ^{99m}Tc-sestamibi patient study contaminated by motion. The short-axis, mid-ventricular images reconstructed from uncorrected projection data show distortion of the LV chamber and artifactual defects in both the anterior and the inferior wall (left). Correcting for motion (center) restores a perfusion pattern qualitatively identical to that seen in images reconstructed from motion-free data (right).

Motion detection and correction using a point source marker on the patient's sternum requires a multi-detector camera to derive source motion in the angular range "shadowed" by the patient. Our implementation used a triple-detector camera, but it is also applicable to a dual-detector camera with any arbitrary angle between its two detectors. For a 90° angle (a preferred choice for 180° reconstruction without attenuation correction in cardiac studies), Equation 4 would translate into:

$$\Delta x_3 = \Delta x_2 \frac{\cos(90° - \phi)}{\cos \phi} \qquad \phi \in (0°, 45°), \quad \text{Eq. 6}$$

where Detector 1 is obviously not present in a dual-detector camera.

CONCLUSIONS

We have proposed a technique that fully detects and corrects translational patient motion in static or dynamic myocardial SPECT studies by using a multi-detector camera and a low-activity ^{99m}Tc point source marker. The algorithm on which this method is based was tested by digitally shifting projection data from phantom experiments and then reconstructing the shifted and the original data as well as the shifted data after correction. For clinical data, visual evaluation of reconstructed images demonstrated that artifactual perfusion defects and image deformation caused by actual motion in human ^{99m}Tc-sestamibi or ^{99m}Tc-teboroxime studies were virtually eliminated by application of our method. The extent to which patient motion coincides with organ motion depends on a variety of factors, including duration of the respiratory cycle and its relation to data acquisition time at any projection angle, respiratory patterns (shallow versus deep breathing) and method of stressing (exercise versus pharmacologic). In any case, correction for gross patient motion should be performed before addressing natural heart motion. Our method involves negligible additional dose to the patient, no deterioration of image quality or lengthening of the procedure, and is capable of correcting motion with accuracy of ±0.37 and ±0.44 mm in the axial and transaxial direction, respectively. In addition, it is compatible with continuous, pseudo-continuous and step and shoot acquisition protocols (*19*).

We have not performed a quantitative or qualitative assessment of the changes in sensitivity and specificity for ^{99m}Tc-sestamibi or ^{99m}Tc-teboroxime myocardial SPECT studies as a function of the degree of simulated motion. In the literature, false-positive findings between 5% (*22*) and 40% (*21*) were reported for a 6.5-mm simulated axial motion in the middle of ^{201}Tl static SPECT studies, i.e., about one and a half times the FWHM of the axial motion com-

ponent measured in our ^{99m}Tc-teboroxime patient population. However, it should be considered that motion-induced artifacts in ^{99m}Tc SPECT studies are probably more severe than analog artifacts in ^{201}Tl SPECT studies for the same amount of motion and the same pre-processing/reconstruction filter cutoff, given the higher resolution capabilities of technetium-based agents. Conversely, we have not performed a quantitative or qualitative assessment of the changes in sensitivity and specificity for ^{99m}Tc-sestamibi or ^{99m}Tc-teboroxime myocardial SPECT studies following the application of our motion correction method. Future extensions of this preliminary work will include validation of the technique in a prospective patient population using quantitative analysis to clearly assess the clinical significance of this motion correction strategy.

ACKNOWLEDGMENTS

The authors thank Diane Martin for the art work in Figure 3 and Dr. Walter Palmas for his help. This work was supported in part by a Picker Graduate Fellowship in Medical Imaging (P.B.K.).

REFERENCES

1. DePuey EG, Garcia EV. Optimal specificity of thallium-201 SPECT through recognition of imaging artifacts. *J Nucl Med* 1992;30:441–449.
2. Eisner R, Churchwell A, Noever T, et al. Quantitative analysis of the tomographic thallium-201 myocardial bullseye display: critical role of correcting for patient motion. *J Nucl Med* 1988;29:91–97.
3. Botvinick EH, Zhu YY, O'Connell WJ, Dae MW. A quantitative assessment of patient motion and its effect on myocardial perfusion SPECT images. *J Nucl Med* 1993;34:303–310.
4. Friedman J, Berman DS, Van Train K, et al. Patient motion in thallium-201 myocardial SPECT imaging: an easily identified frequent source of artifactual defect. *J Nucl Med* 1988;13:321–324.
5. Oppenheim BE. A method using a digital computer for reducing respiratory artifact on liver scans made with a camera. *J Nucl Med* 1971;12:625–628.
6. Hoffer PB, Oppenheim BE, Sterling ML, Yasillo NJ. A simple device for reducing motion artifacts in gamma camera imaging. *Radiology* 1972;103: 199–200.
7. McKeighen RE. Improved means of correcting motion blurring in scintigraphic images. *Phys Med Biol* 1979;24:353–362.
8. Wilson MA, Gaines BS. Correction of respiratory motion in hepatic scintigraphy. *Clin Nucl Med* 1981;6:372–374.
9. Schmidlin P. Development and comparison of computer methods for organ motion correction in scintigraphy. *Phys Med Biol* 1975;20:465–476.
10. Fleming JS. A technique for motion correction in dynamic scintigraphy. *Eur J Nucl Med* 1984;9:397–402.
11. De Agostini A, Moretti R, Belletti S, Maira G, Magri GC, Bestagno M. A motion correction algorithm for an image realignment programme useful for sequential radionuclide renography. *Eur J Nucl Med* 1992;19:476–483.
12. Groch MW, Erwin WD, Turner DA, Domnanovich JR. Dual-isotope motion correction for gated exercise scintigraphy. *J Nucl Med* 1985;26:1478–1484.
13. Potts JM, Borges-Neto S, Smith LR, Jones RH. Comparison of bicycle and treadmill radionuclide angiocardiography. *J Nucl Med* 1991;32:1918–1922.
14. Friedman J, Van Train K, Maddahi J, et al. "Upward creep" of the heart: a frequent source of false-positive reversible defects during thallium-201 stress-redistribution SPECT. *J Nucl Med* 1989;30:1718–1722.
15. Mester J, Weller R, Clausen M, et al. Upward creep of the heart in exercise thallium-201 single photon emission tomography: clinical relevance and a simple correction method. *Eur J Nucl Med* 1991;18:184–190.
16. Eisner RL, Noever T, Nowak D, et al. Use of cross-correlation function to detect patient motion during SPECT imaging. *J Nucl Med* 1987;28:97–101.
17. Geckle WJ, Frank TL, Links JM, Becker LC. Correction for patient and organ movement in SPECT: application to exercise thallium-201 cardiac imaging. *J Nucl Med* 1988;29:441–450.
18. Chua T, Kiat H, Takemoto K, et al. Back to back adenosine teboroxime myocardial perfusion imaging: accuracy and optimal imaging time [Abstract]. *J Nucl Med* 1992;33:854.
19. Germano G, Van Train K, Garcia E, et al. Quantitation of myocardial perfusion with SPECT: current issues and future trends. *Nuclear cardiology: the state of the art and future directions*. St. Louis: Mosby Year Book; 1992:77–88.
20. Garcia EV, Cooke CD, Van Train KF, et al. Technical aspects of myocardial SPECT imaging with technetium-99m sestamibi. *Am J Cardiol* 1990;66: 23E–31E.
21. Eisner RL. Sensitivity of SPECT thallium-201 myocardial perfusion imaging to patient motion. *J Nucl Med* 1992;33:1571–1573.
22. Cooper JA, Neumann PH, McCandless BK. Effect of patient motion on tomographic myocardial perfusion imaging. *J Nucl Med* 1992;33:1566–1571.

EDITORIAL

Effect of Motion on Cardiac SPECT Imaging

There are several major theoretical problems with cardiac SPECT imaging: attenuation, scattering, changes in biodistribution during acquisition, changes in resolution with depth, nonuniformity and nonlinearity of the detector(s), errors in the center-of-rotation, and so forth. Two articles in this issue discuss another problem: motion during acquisition. There are two categories of motion during SPECT acquisition. The whole patient can translate or rotate with respect to the camera or the heart or surrounding organs can move with respect to the rest of the body. An example of the second type of motion is "upward creep" of the heart after exercise, which is probably caused by changes in respiration (*1*). It is truly remarkable to me that with all of these theoretical problems, cardiac SPECT imaging has become a useful clinical tool.

The process of tracking an object in an image is a frequent image processing operation used in tasks as disparate as Landsat imagery, cruise missile navigation and radiologic image registration. The methods in the papers by Germano et al. (*2*) and Cooper et al. (*3*) in this issue represent two general approaches: tracking a fiducial mark or tracking a feature in the image. Fiducial marks can be designed so that they can be accurately and reliably tracked, however, as in myocardial imaging, it is not always possible to affix a fiducial marker to the object of interest.

Germano et al. use a point source on the sternum as a fiducial marker to track and correct for whole-body motion. Cooper et al. track the image of the heart, which tracks both motion of

Received May 6, 1993; revision accepted May 6, 1993.

For correspondence or reprints contact: J. Anthony Parker, MD, PhD, Beth Israel Hospital, Division of Nuclear Medicine, 330 Brookline Ave., Boston, MA 02215.